

# Autocatalytic Behavior of Trimethylindium during Thermal Decomposition

Anthony H. McDaniel\* and Mark D. Allendorf

Combustion Research Facility, Sandia National Laboratories, Livermore, California 94551

Received August 4, 1999. Revised Manuscript Received October 29, 1999

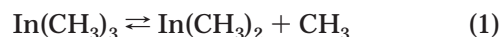
Pyrolysis of trimethylindium (TMIn) in a hot-wall flow-tube reactor has been investigated at temperatures between 573 and 723 K using a modulated molecular-beam mass-sampling technique and detailed numerical modeling. The TMIn was exposed to various mixtures of carrier gases: He, H<sub>2</sub>, D<sub>2</sub>, and C<sub>2</sub>H<sub>4</sub>, in an effort to elucidate the behavior exhibited by this compound in different chemical environments. The decomposition of TMIn is a heterogeneous, autocatalytic process with an induction period that is carrier-gas dependent and lasts on the order of minutes. After activation of the tube wall, the thermolysis exhibits a steady-state behavior that is surface mediated. This result is contrary to prior literature reports, which state that decomposition occurs in the gas phase via successive loss of the CH<sub>3</sub> ligands. This finding also suggests that the bond dissociation energy for the (CH<sub>3</sub>)<sub>2</sub>In–CH<sub>3</sub> bond derived from flow-tube investigations is erroneous and should be reevaluated.

## I. Introduction

Metalorganic chemical vapor deposition (MOCVD) is a key process in the manufacture of groups IIIA–VA advanced optoelectronic materials, such as ternary and quaternary multijunction solar cells, photodiodes, photodetectors, and tunable diode lasers.<sup>1–4</sup> Of particular relevance to the MOCVD community is an understanding of the reactivity and thermal stability of the group IIIA organometallic precursors, the most widely used of which are the trimethyl–alkyls of aluminum (TMAI), gallium (TMGa), and indium (TMIn).<sup>2</sup> For TMIn in particular, the currently held principles regarding thermal stability and mechanisms for decomposition date back to the seminal paper authored by Jacko and Price 35 years ago.<sup>5</sup> Few if any reports on this subject disagree with their original findings that the decomposition of TMIn is initiated by homolytic fission of the metal–carbon bond.

The early observations of Jacko and Price spawned several investigations into the energetics of the metal–carbon bond scission process for TMIn, with the majority of experimentalists using hot-wall flow-tube reactors to conduct their research.<sup>6–8</sup> These investigators endorsed two primary assumptions put forth by Jacko and Price: (1) the decomposition process in the flow reactor is entirely homogeneous and is initiated by the loss of the

first methyl ligand,



and (2), below a certain temperature, reaction 1 is rate limiting. As a result of these hypotheses, the bond dissociation energy (BDE) for the (CH<sub>3</sub>)<sub>2</sub>In–CH<sub>3</sub> bond has been equated to the activation energy for reaction 1 extracted from flow-reactor data,<sup>9,10</sup> thereby establishing the metric of thermal stability for TMIn.

Given the apparent simplicity of this chemical system, it is surprising to note the uncertainty that permeates the literature regarding reaction pathways and the energetics of bond scission. Since Jacko and Price published their results, there have been four reports documenting a complex pyrolytic behavior that is dependent upon the carrier-gas composition.<sup>6,7,11,12</sup> Specifically, investigators have observed a slower rate of TMIn decomposition in inert carriers such as He or N<sub>2</sub> than in H<sub>2</sub>. They have also reported the existence of surface deposits, either carbonaceous or metallic, within the flow tubes such that repeatable observations could only be achieved in *seasoned* vessels. These experimental anomalies result in an inconsistent determination of the activation energy for reaction 1, where values that range from 36 to 54 kcal mol<sup>-1</sup> have been reported.<sup>5–8,13</sup> In addition, they also have fueled a debate regarding the extent to which secondary gas-phase reactions accelerate the decomposition of TMIn.

These discrepant experimental observations are further burdened by the results of recent theoretical work. Quantum-level calculations predicting thermochemical properties, such as BDEs and heats of formation ( $\Delta H_f^\circ$ ),

(1) Davis, R. F. *Proc. IEEE* **1991**, 79, 702.  
 (2) Moon, R. L.; Houg, Y.-M. Organometallic Vapor Phase Epitaxy of III–V Materials. In *Chemical Vapor Deposition*; Hitchman, M. L., Jensen, K. F., Eds.; Academic Press: San Diego, 1993; p 245.  
 (3) Ashley, T. *Inst. Phys. Conf. Ser.* **1995**, 144, 345.  
 (4) Hafizi, M. *Inst. Phys. Conf. Ser.* **1996**, 145, 631.  
 (5) Jacko, M. G.; Price, S. J. W. *Can. J. Chem.* **1964**, 42, 1198.  
 (6) Larsen, C. A.; Stringfellow, G. B. *J. Cryst. Growth* **1986**, 75, 247.  
 (7) Buchan, N. I.; Larsen, C. A.; Stringfellow, G. B. *J. Cryst. Growth* **1988**, 92, 591.  
 (8) Sugiyama, M.; Kusunoki, K.; Shimogaki, Y.; Sudo, S.; Nakano, Y.; Nagamoto, K.; Sugawara, K.; Tada, K.; Komiyama, H. *App. Surf. Sci.* **1997**, 117, 746.

(9) Clark, W. D.; Price, S. J. W. *Can. J. Chem.* **1968**, 46, 1633.  
 (10) Russell, D. K. *Chem. Vap. Deposition* **1996**, 2, 223.  
 (11) Haigh, J.; O'Brien, S. *J. Cryst. Growth* **1984**, 67, 75.  
 (12) Haigh, J.; O'Brien, S. *J. Cryst. Growth* **1984**, 68, 550.  
 (13) Allendorf, M. D.; McDaniel, A. H. *Mater. Res. Soc. Symp. Proc.* **1998**, 495, 125.

have recently been published for TMI<sub>n</sub> and support a much stronger (CH<sub>3</sub>)<sub>2</sub>In-CH<sub>3</sub> bond energy for this compound. The most accurate ab initio molecular orbital and density functional calculations published to date for indium compounds indicate that the BDE for the (CH<sub>3</sub>)<sub>2</sub>In-CH<sub>3</sub> bond is 10–15 kcal mol<sup>-1</sup> stronger than the largest value (54 kcal mol<sup>-1</sup>) ever extracted from flow-tube investigations.<sup>14</sup> Although the accuracy of these calculations for indium-containing compounds is difficult to establish due to a lack of reliable experimental data, the ab initio methods produce results which are in good agreement with values accepted for the simple chlorides InCl<sub>3</sub> and InCl. In addition, agreement between calculated and experimental energetics for group IIIA compounds higher in the periodic table is good. Thus, the validity of the experimental methods must be called into question.

Taking into account the degree of variability in the experimental observations, and the large differences between measured and predicted bond strengths, it is our belief that the analyses of all hot-wall flow-tube data reported thus far for TMI<sub>n</sub> are flawed. The deleterious influences of carrier-gas effects and heterogeneous reactions result in an unreliable measurement of the activation energy for reaction 1. Therefore, in an effort to better understand the behavior of TMI<sub>n</sub> in flow-tube reactors, we investigated the pyrolysis of this compound in various chemical environments using modulated molecular-beam mass spectrometry and detailed numerical modeling. The experimental evidence suggests that TMI<sub>n</sub> decomposition in this type of reactor is preceded by a short induction period indicative of an autocatalytic process. After activation of the tube walls, the thermolysis exhibits a limiting or steady-state behavior that is *completely* surface mediated. To our knowledge, these observations have not been reported for the TMI<sub>n</sub> system, indicating that current mechanisms for pyrolysis in flow-tube reactors are incorrect, as are the energetics of bond cleavage derived from these experiments.

## II. Experimental Section

**Apparatus and Measurements.** The experimental apparatus is described in detail elsewhere.<sup>13,15</sup> It consists of a high-temperature flow reactor (HTFR) comprising a water-jacketed steel vacuum chamber that contains alumina- and graphite-felt insulation, resistive heating elements, and a flow tube interfaced to a molecular-beam mass spectrometer. The essential elements of the system are a quartz flow tube 6.4 cm in diameter and 112 cm in length, a water-jacketed translating injector for admission of thermally sensitive reactants, a differentially pumped vacuum manifold for extraction of gas samples, and a quadrupole mass spectrometer (Extrell C50) with better than unit resolution up to 500 amu. Mass flow controllers are used to meter all gas feed rates. The reactor exhaust is throttled, allowing for feedback control of the reactor pressure to any desired set point within the range of 1–760 Torr. Power to the heating elements is also under feedback control, which provides for a stable centerline temperature that is ±2 K about the set point over 80% of the heated length. Residence times in excess of 2 s can be achieved by adjusting the injector position, total flow rate, pressure, and temperature.

(14) Allendorf, M. D.; Melius, C. F.; Baushlicher, C. W. J. *J. Phys. IV* **1999**, 9, PR8–23.

(15) McDaniel, A. H.; Allendorf, M. D. *J. Phys. Chem. A* **1998**, 102, 7804.

Gases exiting the flow tube are sampled using a molecular-beam expansion through a small orifice that is located within the last 4 cm of the quartz tube. The flow exiting the orifice is supersonic and underexpanded, creating a rotationally cold and collisionless neutral beam that is subsequently chopped by a resonant modulator driven at 800 Hz and ionized by electron impact at 24 eV. The ion signals from the electron multiplier are collected in either one of two modes: (1) the amplified output is directed through an A/D board and digitized continuously as the experiment proceeds (these data will be referred to as analog ion signals); (2) the chopper reference and electron multiplier signals are routed through a lock-in amplifier where the modulated ion signals are extracted from the DC baseline. This allows for discrimination between beam gases and background gases that are present in the quadrupole chamber, thereby increasing the sensitivity of the instrument. These data will be referred to as modulated ion signals. The analog mode is used for fast data-tracking at rates greater than 50 Hz per mass channel, while the modulated mode is used for quantifying gas-phase concentrations of product and reactant species and is limited to data collection rates of 1–5 Hz per mass channel.

The pyrolysis of TMI<sub>n</sub> was investigated at 573, 673, and 723 K in carrier-gas mixtures of He, H<sub>2</sub>, D<sub>2</sub>, C<sub>2</sub>H<sub>4</sub>, and a trace amount of Ar at a total pressure of 15 Torr. The chemical injector was held at a fixed position within the reactor, while the total gas flow rate was adjusted to maintain a constant residence time of 0.3 s in the hot zone. TMI<sub>n</sub> (Epichem) was fed from a manufacturer-supplied bubbler via He carrier gas and diluted to an initial mole fraction of  $(8.5 \pm 0.3) \times 10^{-4}$ . The temperature and back-pressure within the bubbler unit were actively controlled such that the delivery rate of TMI<sub>n</sub> was stable and constant throughout the investigation. Prior to the introduction of TMI<sub>n</sub>, the reactor tube was cleaned at 873 K with a gas mixture containing 3% HCl for 15 min; this was necessary to remove deposits of indium compounds from previous runs.

Experiments were conducted by introducing TMI<sub>n</sub> into the reactor through the injector and monitoring ion signals as a function of time at *m/e* ratios of 150, 145, 115, 40, 30, 17, and 16, which correspond respectively to the ions InCl<sup>+</sup>, C<sub>2</sub>H<sub>6</sub>In<sup>+</sup> (a marker for TMI<sub>n</sub>), In<sup>+</sup>, Ar<sup>+</sup>, C<sub>2</sub>H<sub>6</sub><sup>+</sup>, CH<sub>3</sub>D<sup>+</sup>, and CH<sub>4</sub><sup>+</sup>. All ion signals were normalized to an internal standard of argon in order to minimize the effects of gas composition on recorded signals, which proves to be an effective method for extracting quantitative information from beam studies.<sup>15,16</sup> Mass flow controllers attached to pure gas sources were used to calibrate the system for C<sub>2</sub>H<sub>6</sub> and CH<sub>4</sub>. The same calibration factors measured for CH<sub>4</sub> were used to quantify the CH<sub>3</sub>D ion signals.

**Numerical Method.** In addition to the experimental work, a numerical model was used to further investigate the nature of the surface-mediated steady-state behavior of TMI<sub>n</sub> in our reactor. To simulate the fluid dynamics and chemistry of the flow tube, we used the CRESLAF<sup>17,18</sup> and CHEMKIN<sup>19</sup> software packages. CRESLAF is a FORTRAN program that predicts the velocity, temperature, and species profiles in two-dimensional channels (planar or axisymmetric). The model uses a boundary-layer approximation to solve the coupled hydrodynamic and species continuity equations. As such, there must exist a principal flow direction in which convection

(16) Hsu, W. L.; Tung, D. M. *Rev. Sci. Instrum.* **1992**, 63, 4138.

(17) Coltrin, M.; Kee, R. J.; Miller, J. A. *J. Electrochem. Soc.* **1986**, 133, 1206.

(18) Coltrin, M. E.; Moffat, H. K.; Kee, R. J.; Rupley, F. M. *CRESLAF (Version 4.0): A Fortran Program for Modeling Laminar, Chemically Reacting, Boundary-Layer Flow in Cylindrical or Planar Channels*, SAND93-0478 UC-401; Sandia National Laboratories: Albuquerque, NM, 1996.

(19) Coltrin, M. E.; Kee, R. J.; Rupley, F. M.; Meeks, E.; Miller, J. A. *Chemkin-III: A Fortran Chemical Kinetics Package for the Analysis of Gas-Phase Chemical and Plasma Kinetics and Surface Chemkin-III: A Fortran Package for Analyzing Heterogeneous Chemical Kinetics at a Solid-Surface-Gas-phase Interface* SAND96-8216 UC-405 and SAND96-8217 UC-405; Sandia National Laboratories: Albuquerque, NM, 1996.

dominates diffusive transport, a criteria that is always met under the laminar-flow conditions of these experiments. The model accounts for finite-rate gas-phase and surface chemistries, as well as multicomponent molecular transport, via the CHEMKIN, SURFACE CHEMKIN, and transport interpreters,<sup>20</sup> respectively. These three software packages compose a body of subroutines that are linked to CRESLAF, creating a standard platform from which to calculate equations of state, chemical production rates, thermodynamic properties, and mass diffusivities. For a complete discussion on CRESLAF and the CHEMKIN packages, the reader is referred to the above literature citations and the references cited therein.

The model predictions of species concentration profiles within the reactor were used to calculate the mole fractions of hydrocarbons produced during thermolysis of TMIIn. These predictions were then compared to experimental values measured under various reactor conditions in order to support or refute proposed reaction schemes. Specifically, we wanted to investigate the significance of gas-phase radical reactions during surface-mediated decomposition of TMIIn. The pertinent reaction schemes will be developed in a subsequent section.

### III. Results of HTFR Experiments

To better understand the chemical reactions involved in thermolysis of this important MOCVD precursor, the pyrolytic behavior of TMIIn was investigated at 573, 673, and 723 K in five different carrier-gas compositions: pure He; a 90:10 mix of He:C<sub>2</sub>H<sub>4</sub>; a 50:50 split of He:H<sub>2</sub> or He:D<sub>2</sub>; and a 40:50:10 mix of He:H<sub>2</sub>:C<sub>2</sub>H<sub>4</sub>. Our observations are consistent with previous investigations with regard to the following:<sup>5-8,12</sup> (1) the hydrocarbon products formed during pyrolysis, primarily CH<sub>4</sub> (or CH<sub>3</sub>D) and C<sub>2</sub>H<sub>6</sub>, (2) the acceleration of TMIIn decomposition in H<sub>2</sub> carrier gas, and (3) the presence of surface deposits within the hot zone of the reactor. However, this work differs from previous investigations in that the initial stages of TMIIn decomposition were closely monitored in order to explicate the role of heterogeneous chemistry. To this end, the reactor tube was always cleaned prior to TMIIn exposure, meaning that pertinent observations were never made in a *seasoned* vessel, as was the case in all previous flow-tube studies.

Illustrated in Figure 1 is an analog scan of the C<sub>2</sub>H<sub>6</sub>In<sup>+</sup> (*m/e* 145) ion signal as a function of time for TMIIn exposures at 573, 673, and 723 K in pure He carrier gas at 15 Torr and at a constant residence time of 0.3 s. At 573 K, the TMIIn ion signal reaches a constant value shortly after its introduction into the reactor. This condition serves as a signal baseline and represents an unreactive state. At 673 K the signal behavior is quite different; the ion trace attains the same value as the unreactive state for approximately 5 min, then decreases over a period of several minutes, and plateaus at times longer than 14 min. The signal level at the plateau indicates that approximately 60% of the TMIIn has decomposed. For a reactor temperature of 723 K, the TMIIn signal nearly attains the value of the unreactive state but drops quickly to zero, indicating 100% decomposition of the TMIIn.

It is clear from the ion signals in Figure 1 that TMIIn decomposition in flow-tube reactors is preceded by an induction period during which the walls become acti-

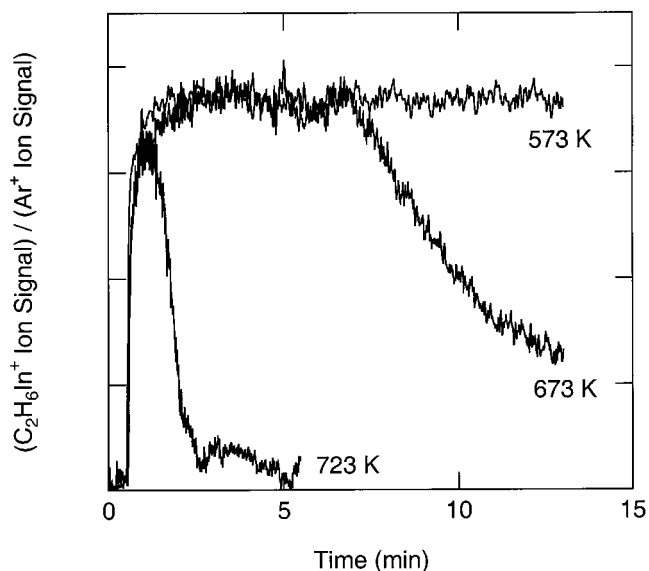


**Figure 1.** Analog scan of the normalized C<sub>2</sub>H<sub>6</sub>In<sup>+</sup> (*m/e* 145) ion signal as a function of reaction time at 573, 673, and 723 K for a constant residence time of 0.3 s in He carrier gas at 15 Torr. TMIIn is introduced into the reactor at 0.5 min.

vated. The chemical composition of the active surface likely contains indium and perhaps carbonaceous material in the form of CH<sub>x</sub> groups, which has been suggested in the past.<sup>6,7</sup> The results of our tube-cleaning procedure substantiate these assumptions. Shown in Figure 2 are the analog scans of the CH<sub>4</sub><sup>+</sup>/CH<sub>2</sub>D<sup>+</sup> (*m/e* 16) and InCl<sup>+</sup> (*m/e* 150) ion signals as a function of time during exposure to a gas flow containing 3% HCl in pure He. These data were collected after a typical experiment and serve to identify the nature of the deposits found on the tube wall following TMIIn decomposition. Gas flows containing TMIIn and D<sub>2</sub> were discontinued for a period of at least 5 min prior to HCl addition in order to ensure complete purging of these compounds from the reactor vessel.

With reference to Figure 2, HCl was added to the carrier flow at 0.4 min, at which time a ramp in the reactor temperature from 673 to 873 K was initiated. When HCl is first introduced into the reactor, CH<sub>4</sub> and a chloride of indium (InCl<sub>x</sub>, *x* = 1, 2, 3) are seen in the exhaust gases. No mass peaks are observed above 150 amu; however, the *m/e* 150 mass feature cannot be definitively assigned to the sub-chloride InCl without further knowledge of the fragmentation pattern of the other chlorides (*x* = 2, 3). At times between 0.4 and 1.5 min, a large burst of InCl<sub>x</sub> is coincident with the CH<sub>4</sub> peak, after which the CH<sub>4</sub> vanishes and the InCl<sub>x</sub> signal drops by a factor of 3. The reactor temperature reaches 873 K at approximately 5 min, where the InCl<sub>x</sub> feature peaks and then gradually drops to zero. The data in Figure 2 indicate that stable surface species persist on the tube wall after TMIIn exposure at 673 K and may be volatilized by adding HCl and heating the reactor to 873 K.

There appear to be at least two types of adsorbates on the reactor walls that can be identified by reaction with HCl, one containing the CH<sub>x</sub>In (*x* = 1, 2, 3) group and the other indium. The sharp drop in the InCl<sub>x</sub> signal at 1.5 min may suggest a transition from removal of adsorbed CH<sub>x</sub>In groups to the removal of bulk indium,

(20) Kee, R. J.; Dixon-Lewis, G.; Warnatz, J.; Coltrin, M. E.; Miller, J. A. *A Fortran Computer Code Package for the Evaluation of Gas-Phase Multicomponent Transport Properties*, SAND86-8246 UC-32; Sandia National Laboratories: Albuquerque, NM, 1986.

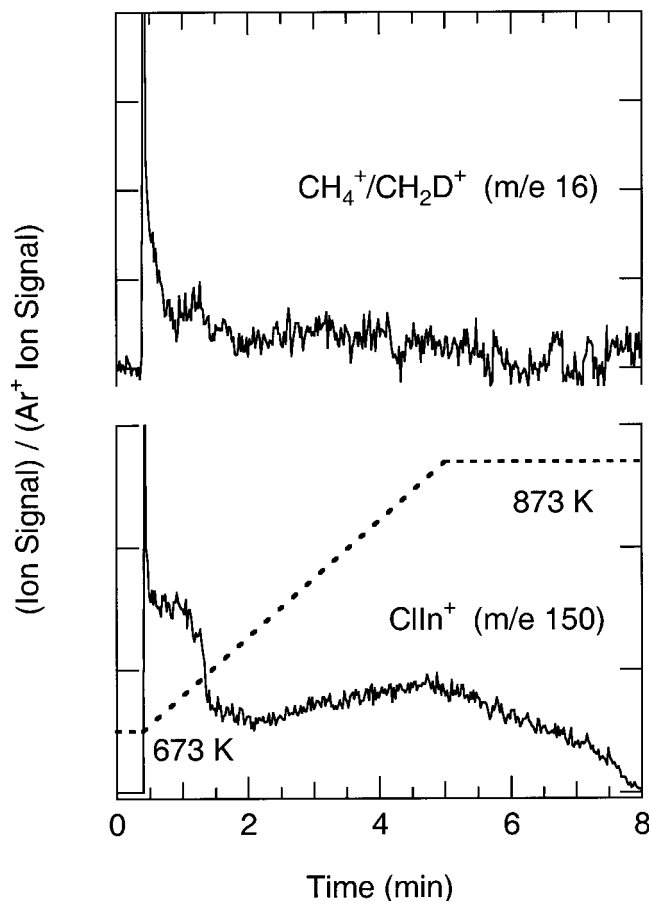


**Figure 2.** Analog scans of the normalized ion signals for  $\text{CH}_4^+/\text{CH}_2\text{D}^+$  ( $m/e$  16) and  $\text{ClIn}^+$  ( $m/e$  150) as a function of etch time taken at the conclusion of a 20 min exposure to TMI in a 50:50 mix of He: $\text{D}_2$ . HCl (3 vol %) is introduced into the reactor at 0.4 min; from 0.4 to 5 min the reactor temperature is ramped from 673 to 873 K (dashed line).

the latter having a greater energy barrier to reaction with HCl than the former. In any event, after the acid etch the quartz reactor is clean and a mixture of white and yellow crystallites (presumably  $\text{InCl}_x$ ) can be found in the colder regions of the exhaust manifold downstream from the flow tube.

**Carrier Gas Effects.** A principal observation of TMI thermolysis is that the relative reactivity of the carrier gas changes the apparent rate of decomposition. Shown in Figure 3 are the modulated ion signals for  $\text{C}_2\text{H}_6\text{In}^+$  as a function of time during exposure to TMI at 673 K in various carrier-gas environments. Listed in Table 1 are the induction times and the steady-state conversions of TMI for each of the reactor conditions investigated. The length of the induction period was calculated from the time difference between the points at which the TMI and  $\text{C}_2\text{H}_6$  signals began to depart from the baseline, the former indicating the beginning of TMI exposure and the latter indicating that the decomposition rate had increased to a measurable level. Two pertinent observations are apparent in Figure 3 and Table 1. First and foremost, the initial TMI signal always rises to the level of the unreactive state regardless of the carrier-gas composition, and second, switching from pure He to 50:50 mixtures of He: $\text{D}_2$  and then He: $\text{H}_2$  decreases the induction time from 4.6, to 1.3, to 0.3 min with a concomitant increase in the steady-state conversion of TMI from 57, to 82, to 96%, respectively.

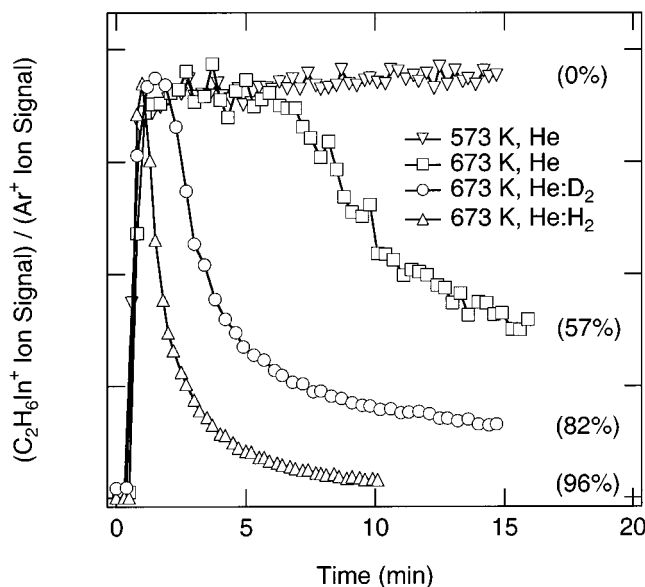


**Figure 3.** Modulated ion signal for  $\text{C}_2\text{H}_6\text{In}^+$  ( $m/e$  145) as a function of reaction time at 573 and 673 K, a constant residence time of 0.3 s, in various carrier-gas compositions at 15 Torr. TMI is introduced into the reactor at 0.5 min. The numbers in parentheses indicate percent conversion at steady state.

**Table 1. Induction Time, Steady-State Conversion, and Hydrocarbon Product Mole Fractions for TMI Pyrolysis as a Function of Carrier-Gas Composition at 673 K, a Reactor Pressure of 15 Torr, and an Initial TMI Mole Fraction of  $(8.5 \pm 0.3) \times 10^{-4}$**

carrier gas	mixing ratio	ind time (min)	conversion (%)	mole fraction $\times 10^{-4}$ <sup>b</sup>	
				$\text{CH}_4$ or $\text{CH}_3\text{D}$	$\text{C}_2\text{H}_6$
He <sup>a</sup>		4.6	57	$0.1 \pm 0.1$	$7.8 \pm 0.3$
He: $\text{D}_2$	50:50	1.3	82	$2.5 \pm 0.1$	$8.5 \pm 0.2$
He: $\text{H}_2$	50:50	0.3	96	$7.1 \pm 0.3$	$8.7 \pm 0.1$
He: $\text{C}_2\text{H}_4$	90:10	2.3	62	$0.2 \pm 0.1$	$7.1 \pm 0.2$
He: $\text{H}_2$ : $\text{C}_2\text{H}_4$	40:50:10	1.2	89	$5.3 \pm 0.3$	$7.7 \pm 0.3$

<sup>a</sup> Decomposition of TMI in He carrier gas is not at steady-state after 15 min of reaction (see text). <sup>b</sup> The reported uncertainty is based upon the precision of the measurement at the 95% confidence interval and as such represents the scatter in the data.

The composition of the carrier gas also affects the distribution of hydrocarbon products formed during TMI pyrolysis. Figure 4 illustrates the time-dependent behavior of the mole fractions for  $\text{C}_2\text{H}_6$ ,  $\text{CH}_4$ , and  $\text{CH}_3\text{D}$  measured during TMI exposure at 673 K. Here,  $\text{C}_2\text{H}_6$  is the only gas-phase product of consequence formed in pure He. Upon the addition of  $\text{H}_2$  ( $\text{D}_2$ ),  $\text{CH}_4$  ( $\text{CH}_3\text{D}$ ) is produced in addition to  $\text{C}_2\text{H}_6$ . The delay in the onset of hydrocarbon production is coincident with the break point of the TMI signals in Figure 3, which emphasizes the strong correlation between  $\text{C}_2\text{H}_6\text{In}^+$  ion signals (TMI marker) and the progress of the decomposition reaction. The large spike of short duration in the  $\text{CH}_4$  signal for the He and He: $\text{H}_2$  cases in Figure 4 is due to the accumulation of  $\text{CH}_4$  in the source bubbler and not to chemical reactions occurring within the flow tube. The absence of a spike in the  $\text{CH}_3\text{D}$  signal (filled circles,  $m/e$  17) supports this notion because this compound is not a byproduct of TMI decomposition within the bubbler.

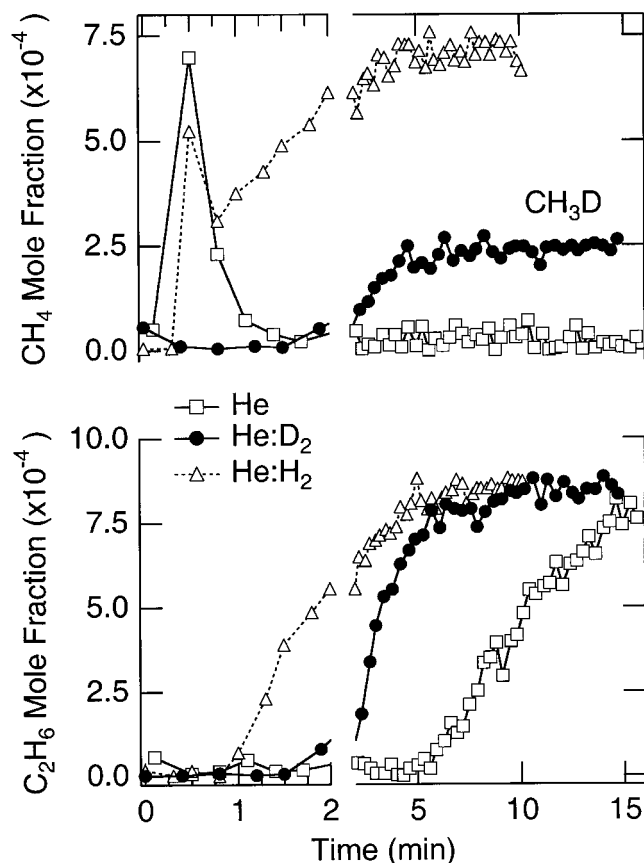


**Figure 4.** Mole fractions of  $\text{CH}_4$  (or  $\text{CH}_3\text{D}$ ) and  $\text{C}_2\text{H}_6$  measured as a function of reaction time at 673 K, with a constant residence time of 0.3 s, and in various carrier-gas compositions at 15 Torr. The abscissa has been expanded below 2 min in order to resolve early transients.

Listed in Table 1 are the steady-state values of the hydrocarbon mole fractions taken from the data in Figure 4. It is evident that the limiting or steady-state mole fraction of  $\text{C}_2\text{H}_6$ , which averages  $(8.3 \pm 0.5) \times 10^{-4}$  for decomposition in the absence of  $\text{C}_2\text{H}_4$ , is nearly independent of the carrier-gas composition. Conversely, the formation of  $\text{CH}_4$  or  $\text{CH}_3\text{D}$  is a direct result of adding  $\text{H}_2$  or  $\text{D}_2$  and is thereby dependent on the carrier-gas composition. In addition, the amount of  $\text{CH}_3\text{D}$  formed during decomposition in  $\text{He}:\text{D}_2$  is a factor of 3 less than the amount of  $\text{CH}_4$  produced in  $\text{He}:\text{H}_2$ . This correlates well with the lower steady-state conversion of TMIn in  $\text{He}:\text{D}_2$  mixtures and is most likely the result of a kinetic isotope effect.

**Ethylene Addition.** A natural hypothesis that can be proposed from the observed pyrolysis behavior of TMIn in  $\text{H}_2$  ( $\text{D}_2$ ) is that the additional chemistry is driven by reactions of gas-phase  $\text{CH}_3$  and  $\text{H}$  radicals with  $\text{H}_2$  ( $\text{D}_2$ ). These processes are well-documented within the combustion literature and can certainly account for the formation of  $\text{CH}_4$  in  $\text{H}_2$ ,<sup>21</sup> as well as the acceleration of TMIn decomposition, provided that these reactions are initiated and then further propagated in the gas phase.

To test this hypothesis we added  $\text{C}_2\text{H}_4$  (10 vol %), which effectively converts  $\text{H}$  and  $\text{CH}_3$  to longer-chain radicals ( $\text{C}_2\text{H}_5$  and  $\text{C}_3\text{H}_7$ ) by insertion into the carbon-

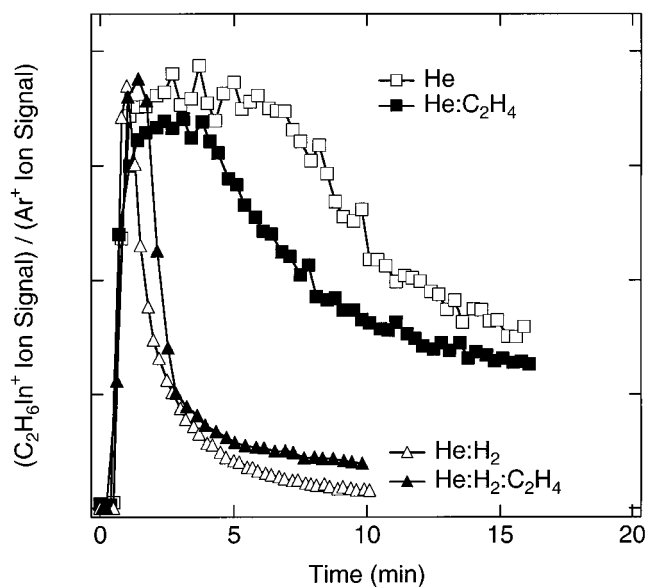


**Figure 5.** Modulated ion signal for  $\text{C}_2\text{H}_6\text{In}^+$  ( $m/e$  145) as a function of reaction time at 673 K, with a constant residence time of 0.3 s, in various carrier-gas compositions at 15 Torr. TMIn is introduced into the reactor at 0.5 min.

carbon double bond,<sup>22,23</sup> to the carrier flow for TMIn pyrolysis in pure He and a mixture of  $\text{He}:\text{H}_2$ . Presented in Figure 5 are the modulated ion signals for  $\text{C}_2\text{H}_6\text{In}^+$  as a function of time during exposure to TMIn at 673 K in pure He, a 90:10 mixture of  $\text{He}:\text{C}_2\text{H}_4$ , a 50:50 mixture of  $\text{He}:\text{H}_2$ , and a 40:50:10 mixture of  $\text{He}:\text{H}_2:\text{C}_2\text{H}_4$ . It is readily apparent from the ion signals that the presence of  $\text{C}_2\text{H}_4$  affects the length of the induction period for both the He and  $\text{He}:\text{H}_2$  cases (see Table 1). The induction time decreases by a factor of 2 relative to that in He and increases by a factor of 4 relative to the time observed for the  $\text{He}:\text{H}_2$  mixture. The data in Table 1 also indicate that  $\text{C}_2\text{H}_4$  exerts a minor influence (changes of order less than 10%) on the steady-state conversion of TMIn. However, the initial thermal stability of TMIn has not been altered, as evidenced by the maximum in the  $\text{C}_2\text{H}_6\text{In}^+$  ion signals for each experiment, which are all approximately the same intensity and equal to that of the unreactive condition (573 K, He ambient).

The addition of  $\text{C}_2\text{H}_4$  also changes the hydrocarbon product distribution, as evidenced by the data presented in Table 1. The steady-state mole fractions for  $\text{C}_2\text{H}_6$  decrease by roughly 11% for each case, while the production of  $\text{CH}_4$  in He versus  $\text{He}:\text{C}_2\text{H}_4$  remains unchanged within the experimental uncertainty. The largest effect of  $\text{C}_2\text{H}_4$  addition can be seen on the amount of  $\text{CH}_4$  measured in a  $\text{He}:\text{H}_2$  mix versus the 40:50:10 split of  $\text{He}:\text{H}_2:\text{C}_2\text{H}_4$ , where the amount of  $\text{CH}_4$  decreases by 25%. In addition to a decrease in the amount of  $\text{C}_1$  and  $\text{C}_2$  hydrocarbons produced, we also observed the appearance of mass peaks at  $m/e$  of 44 and 43, which correspond to longer-chain  $\text{C}_3$  and  $\text{C}_4$  moieties. No attempt was made to quantify the amount of  $\text{C}_3$  and  $\text{C}_4$  produced in these experiments, but it was noted that the relative intensities of the  $m/e$  44 and 43 signals were greater in the presence of  $\text{H}_2$  than in the  $\text{He}:\text{C}_2\text{H}_4$  experiment.

(21) Marinov, N. M.; Pitz, W. J.; Westbrook, C. K.; Castaldi, M. J.; Senkin, S. M. *Combust. Sci. Technol.* **1996**, *116*, 211.

(22) Tsang, W.; Hampson, R. F. *J. Chem. Ref. Data* **1986**, *15*, 1087.  
(23) Holt, P. M.; Kerr, J. A. *Int. J. Chem. Kinet.* **1977**, *9*, 185.

**Table 2. Global Surface Reaction Mechanisms Used to Simulate the Effects of Carrier-Gas Composition on Steady-State TMIn Pyrolysis at 673 K and 15 Torr**

no.	global surface reactions <sup>a</sup>	A	$\beta$	E <sup>b</sup>
S1	$\text{In}(\text{CH}_3)_3 + \text{In}(\text{s}) \rightarrow \frac{1}{2}(3-x)\text{C}_2\text{H}_6 + x\text{CH}_3 + \text{In}(\text{s}) + \text{In}(\text{b})$	$2.07 \times 10^{13}$	-0.5	46 170
S2	$\text{In}(\text{CH}_3)_3 + \text{In}(\text{s}) \rightarrow \frac{1}{2}(3-x)\text{C}_2\text{H}_6 + x\text{CH}_3 + \text{In}(\text{s}) + \text{In}(\text{b})$	$2.07 \times 10^{13}$	-0.5	44 170
S3	$\text{In}(\text{CH}_3)_3 + \text{In}(\text{s}) \rightarrow (\text{CH}_3)_3\text{In}(\text{s}) + \text{In}(\text{b})$	1.0	0.0	0.0
	$(\text{CH}_3)_3\text{In}(\text{s}) \rightarrow \frac{1}{2}(3-x)\text{C}_2\text{H}_6 + x\text{CH}_3 + \text{In}(\text{s})$	$6.20 \times 10^{14}$	0.0	46 170
	$\frac{1}{2}\text{H}_2 + \frac{1}{3}(\text{CH}_3)_3\text{In}(\text{s}) \rightarrow \text{CH}_4 + \frac{1}{3}\text{In}(\text{s})$	$1.00 \times 10^{13}$	-0.5	57 000

<sup>a</sup> Surface-phase rate constant of the form  $\gamma = AT^b \exp[-E/RT]$  which is unitless and in the range ( $0 \leq \gamma \leq 1$ ); s = surface and b = bulk species. <sup>b</sup> Units of calorie per mole.

**Summary of HTFR Experiments.** While earlier investigators have documented the relative increase in the apparent rate of TMIn decomposition in H<sub>2</sub> (D<sub>2</sub>) ambients,<sup>6,7,12</sup> as well as the change in hydrocarbon product distribution,<sup>6,7</sup> they did not describe any transient behaviors of TMIn pyrolysis in their flow-tube reactors. Our experimental observations indicate that thermal decomposition of TMIn is a process involving complex heterogeneous reactions. An initial incubation period is followed by an exponential increase in the consumption of TMIn which, after a relatively short period of time, exhibits steady-state behavior.

The initial stages of this reaction are affected by the presence of H<sub>2</sub> or D<sub>2</sub> in the carrier gas; these compounds can increase the reactivity of the flow-tube environment by participating in the propagation of radical chain reactions. The addition of H<sub>2</sub> or D<sub>2</sub> to the carrier-gas mixture decreases the induction time relative to the pure He case, increases the rate of TMIn conversion at steady-state, and creates CH<sub>4</sub> or CH<sub>3</sub>D. In addition, the extent of pyrolysis is greatest in mixtures of He:H<sub>2</sub> and decreases in He:D<sub>2</sub>, with the least reactive state observed for pure He carrier gas. Adding C<sub>2</sub>H<sub>4</sub> to perturb the gas-phase radical pool affects the induction times for both He and He:H<sub>2</sub>, creates longer chain alkyls (C<sub>3</sub> and C<sub>4</sub>), presumably indicating the presence of gas-phase CH<sub>3</sub> and H, and decreases by 25% the amount of CH<sub>4</sub> produced in He:H<sub>2</sub> mixtures. The composition of the carrier gas does not, however, affect the initial thermal stability of TMIn nor does it strongly influence the steady-state production rate of C<sub>2</sub>H<sub>6</sub> at 15 Torr and 673 K.

These new results strongly suggest that existing concepts concerning the thermal stability of TMIn, and accepted mechanisms for its decomposition by gas-phase reactions during MOCVD, are likely to be in error. Consequently, past speculation as to the exact nature of carrier-gas effects, specifically the supposition that gas-phase radical reactions are responsible for an increase in the apparent rate of TMIn decomposition, may also be in error. These ideas will be explored numerically in the next section of this paper.

#### IV. Results of Numerical Experiments

The intention of the numerical work is not to address issues related to the transient aspects of surface activation, but instead to focus on the steady-state pyrolysis of TMIn in hot-wall flow-tube environments. Our specific objective is to formulate plausible mechanisms for TMIn decomposition and to evaluate the relative importance of gas-phase radical processes in this system as they pertain to the observed carrier-gas effects and conversion efficiency. To accomplish this task, various

reaction mechanisms are developed, incorporated into the flow model, and then tested by comparing simulated hydrocarbon product distributions to experimental data.

**Mechanism Development.** To model the observed steady-state behavior of TMIn in our flow-tube reactor, we combine irreversible global surface reactions with a comprehensive elementary gas-phase mechanism. The use of global surface reactions maintains the premise that TMIn decomposition is initially heterogeneous, while minimizing the difficulty of resolving thermochemistry and elementary kinetics for a complex surface-mediated process. The net effect is to provide a simple route for conversion of TMIn to hydrocarbons and reactive intermediates, which then desorb into the gas. Once the decomposition products have volatilized, they are free to participate in numerous well-defined abstraction, elimination, initiation, and propagation reactions. This method provides an effective means for investigating the significance of gas-phase radical chemistry and to identify key rate-limiting processes.<sup>15</sup>

Listed in Tables 2 and 3 are the reactions incorporated into the flow model. There are three global surface mechanisms, labeled S1–S3 (Table 2), and two gas-phase mechanisms, labeled G1 and BLS (Table 3). Simulations that combine one surface mechanism with either G1 or BLS were used to test the relative importance of gas-phase and surface chemistries to TMIn decomposition.

The mechanisms S1, S2, and S3 in Table 2 capture the essence of the experimental observations in that TMIn decomposition is entirely heterogeneous. The organometallic molecule impinges onto active indium sites at the surface, and through various elementary reactions that are embodied within one or more global steps, C<sub>2</sub>H<sub>6</sub>, CH<sub>4</sub>, and CH<sub>3</sub> desorb into the gas. The parameter  $x$  in these equations is used to adjust the relative amount of C<sub>2</sub>H<sub>6</sub> versus CH<sub>3</sub> that enters the gas phase. Mechanisms S1 and S2 are identical except for a 2 kcal mol<sup>-1</sup> difference in activation energy. This energy difference accounts for an increase in the surface reactivity induced by hydrogen exposure, which is observed experimentally as a carrier-gas effect, and is possibly due to the formation of surface defects as has been suggested by Bartram and Creighton for MOCVD of GaN.<sup>24</sup> However, reducing the activation energy by 2 kcal mol<sup>-1</sup> does not directly influence the hydrocarbon product distribution nor does it depend on the absolute amount of hydrogen in the system.

In S3, the process of TMIn decomposition occurs in two steps via an alkyl intermediate formed by TMIn adsorption. Here, the surface-bound organometallic

(24) Bartram, M. E.; Creighton, J. R. *Personal communication*, 1999.

**Table 3. Elementary Gas-Phase Reaction Mechanisms Used to Simulate the Effects of Carrier-Gas Composition on Steady-State TMI<sub>n</sub> Pyrolysis at 673 K and 15 Torr**

no.	elementary gas-phase reactions <sup>a</sup>	A	β	E <sup>b</sup>
G1 <sup>c</sup>	H: 11, 11a			
	C <sub>1</sub> : 21–23, 37–39, 101–103			
	C <sub>2</sub> : 64, 75, 76, 79–81, 83, 85, 88, 90, 122, 123, 126–128, 133, 137, 138, 141, 148–151, 153, 155, 167			
	C <sub>2</sub> H <sub>4</sub> (+M) ⇌ C <sub>2</sub> H <sub>2</sub> + H <sub>2</sub> (+M)	1.80 × 10 <sup>13</sup>	0.0	76 000
	low-pressure limit:	1.50 × 10 <sup>15</sup>	0.0	55 443
	C <sub>2</sub> H <sub>3</sub> + H (+M) ⇌ C <sub>2</sub> H <sub>4</sub> (+M)	6.10 × 10 <sup>12</sup>	0.3	280
	low-pressure limit:	9.80 × 10 <sup>29</sup>	-3.86	3 320
	Troe parameters: α = 0.782, T <sup>***</sup> = 208, T* = 2663, T** = 6095			
	C <sub>2</sub> H <sub>3</sub> + C <sub>2</sub> H <sub>3</sub> ⇌ CH <sub>2</sub> CHCHCH <sub>2</sub>	7.13 × 10 <sup>13</sup>	0.0	0.0
	C <sub>3</sub> : 218, 227–237, 240–242, 245, 257–260, 264–266, 288, 292, 299, 300			
	HCCCHCH <sub>3</sub> + H ⇌ C <sub>3</sub> H <sub>6</sub>	1.00 × 10 <sup>14</sup>	0.0	0.0
	CH <sub>2</sub> CCH <sub>3</sub> + H ⇌ C <sub>3</sub> H <sub>6</sub>	5.00 × 10 <sup>13</sup>	0.0	0.0
	C <sub>4</sub> : 342–345, 348, 349, 360–362, 364–368, 372, 374–376, 382, 384, 385, 387			
	CH <sub>3</sub> CHCH <sub>2</sub> CH <sub>3</sub> (+M) ⇌ C <sub>3</sub> H <sub>6</sub> + CH <sub>3</sub> (+M)	2.14 × 10 <sup>12</sup>	0.7	30 856
	low-pressure limit:	6.32 × 10 <sup>58</sup>	-12.85	35 567
	enhanced third-body efficiencies: H <sub>2</sub> = 2.0			
	n-C <sub>4</sub> H <sub>9</sub> (+M) ⇌ C <sub>2</sub> H <sub>5</sub> + C <sub>2</sub> H <sub>4</sub> (+M)	1.06 × 10 <sup>13</sup>	0.0	27 828
	low-pressure limit:	1.90 × 10 <sup>55</sup>	-11.91	32 263
	enhanced third-body efficiencies: H <sub>2</sub> = 2.0			
	n-C <sub>4</sub> H <sub>10</sub> + H ⇌ n-C <sub>4</sub> H <sub>9</sub> + H <sub>2</sub>	2.84 × 10 <sup>5</sup>	2.5	6 050
	n-C <sub>4</sub> H <sub>10</sub> + H ⇌ CH <sub>3</sub> CHCH <sub>2</sub> CH <sub>3</sub> + H <sub>2</sub>	5.68 × 10 <sup>5</sup>	2.4	3 765
	n-C <sub>4</sub> H <sub>10</sub> + CH <sub>3</sub> ⇌ n-C <sub>4</sub> H <sub>9</sub> + CH <sub>4</sub>	5.00 × 10 <sup>11</sup>	0.0	13 600
	n-C <sub>4</sub> H <sub>10</sub> + CH <sub>3</sub> ⇌ CH <sub>3</sub> CHCH <sub>2</sub> CH <sub>3</sub> + CH <sub>4</sub>	4.30 × 10 <sup>11</sup>	0.0	10 500
BLS	G1			
	H + In(CH <sub>3</sub> ) <sub>3</sub> → HIn(CH <sub>3</sub> ) <sub>3</sub>	1.00 × 10 <sup>13</sup>	0.0	0.0
	CH <sub>3</sub> + HIn(CH <sub>3</sub> ) <sub>3</sub> → CH <sub>4</sub> + In(CH <sub>3</sub> ) <sub>3</sub>	1.00 × 10 <sup>13</sup>	0.0	0.0
	H + HIn(CH <sub>3</sub> ) <sub>3</sub> → H <sub>2</sub> + In(CH <sub>3</sub> ) <sub>3</sub>	1.00 × 10 <sup>13</sup>	0.0	0.0
	HIn(CH <sub>3</sub> ) <sub>3</sub> → CH <sub>4</sub> + 2CH <sub>3</sub> + In	2.00 × 10 <sup>9</sup>	0.0	20 000

<sup>a</sup> Gas-phase rate constant of the form  $k = AT^b \exp[-E/RT]$  in units of (cm<sup>3</sup> mol<sup>-1</sup> s<sup>-1</sup> or s<sup>-1</sup>). <sup>b</sup> Units of calorie per mole. <sup>c</sup> Numbers refer to reactions listed in Table 2 of Marinov et al.<sup>21</sup> C<sub>a</sub> (a = 1–4) refers to the number of carbon atoms in the primary reactant. Additional reactions listed here are modifications to the original Marinov mechanism.<sup>38,39</sup>

either decomposes by desorption of alkyls or reacts with H<sub>2</sub> to produce CH<sub>4</sub>. This step provides a direct pathway for accelerating TMI<sub>n</sub> decomposition in the presence of H<sub>2</sub>, via the liberation of an active surface site, that does not rely upon gas-phase intermediates. Here again, the liberation of CH<sub>4</sub> is a concerted process that most likely involves the dissociation of H<sub>2</sub> on the surface to form adsorbed H atoms, which then recombine with alkyl fragments to form CH<sub>4</sub>. We chose to avoid such a detailed description in order to simplify the surface reaction scheme, thereby reducing the number of unknown kinetic constants. The sequences S1 through S3 allow for the consideration that all carrier-gas effects in this system are completely surface mediated.

While the desorption of C<sub>2</sub>H<sub>6</sub> and CH<sub>4</sub> from alkylated metal<sup>25–28</sup> and semiconducting<sup>29,30</sup> surfaces is not without precedent, the desorption of CH<sub>3</sub> under our experimental conditions should be considered further. A large body of supporting literature exists that documents the desorption of CH<sub>3</sub> radical from semiconductor surfaces after exposure to TMGa and TMI<sub>n</sub> under ultrahigh vacuum conditions.<sup>31–35</sup> In fact, temperature-programmed

desorption (TPD) investigations have established methyl loss as a primary route to organometallic decomposition above 650 K. However, the viability of this pathway under MOCVD conditions, which operate at pressures typically in the range of 1–760 Torr where surfaces experience high reactant fluxes, has not been established.

Nonetheless, Butler et al.<sup>36</sup> were able to detect appreciable quantities of CH<sub>3</sub> radical in the boundary layer above heated substrates exposed to TMI<sub>n</sub> using infrared-diode laser spectroscopy in a cold-wall MOCVD apparatus at 7.6 Torr and substrate temperatures below 673 K. Recently, Russell et al.<sup>37</sup> detected the presence of gas-phase CH<sub>3</sub> radicals in a hot-wall pyrolysis chamber using matrix isolation electron spin-resonance (ESR) spectroscopy during the thermolysis of similar group IIIA precursors. Therefore, the desorption of CH<sub>3</sub> under MOCVD conditions seems reasonable.

To describe the gas-phase reactions between unstable intermediates and the stable hydrocarbons and/or carrier gases present in the boundary above the surface, we adopted relevant portions of a hydrocarbon combustion mechanism proposed by Marinov et al. (labeled G1 in Table 3).<sup>21</sup> The subset used here, which borrows from the comprehensive reaction set proposed by Marinov to describe the formation of aromatic and polycyclic aromatic hydrocarbons in fuel-rich methane and ethane flames, contains detailed kinetics and thermodynamics for 97 reversible elementary reactions between He, H,

(35) Wang, H.; Zhu, X. Y.; Xin, Q. S. *J. Vac. Sci. Technol. A* **1998**, *16*, 948.

(36) Butler, J. E.; Bottka, N.; Sillmon, R. S.; Gaskill, D. K. *J. Cryst. Growth* **1986**, *77*, 163.

(37) Russell, D. K.; Mills, G. P.; Raynor, J. B.; Workman, A. D. *Chem. Vap. Deposition* **1998**, *4*, 61.

(25) Lin, J. L.; Bent, B. E. *J. Am. Chem. Soc.* **1993**, *115*, 6943.  
 (26) Lin, J. L.; Chiang, C. M.; Jenks, C. J.; Yang, M. X.; Wentzclaff, T. H.; Bent, B. E. *J. Catal.* **1994**, *147*, 250.  
 (27) Colin, L.; Cassuto, A.; Ehrhardt, J. J.; Ruizlopez, M. F.; Jamois, D. *Appl. Surf. Sci.* **1996**, *99*, 245.  
 (28) Chaturvedi, S.; Strongin, D. R. *Langmuir* **1997**, *13*, 3162.  
 (29) Lin, R.; Masel, R. I. *Surf. Sci.* **1991**, *258*, 225.  
 (30) Cadwell, L. A.; Masel, R. I. *Surf. Sci.* **1994**, *301*, 415.  
 (31) Creighton, J. R. *J. Vac. Sci. Technol. A* **1991**, *9*, 2895.  
 (32) McCaulley, J. A.; Shui, R. J.; Donnelly, V. M. *J. Vac. Sci. Technol. A* **1991**, *9*, 2872.  
 (33) Zhu, X. Y.; White, J. M.; Creighton, J. R. *J. Vac. Sci. Technol. A* **1992**, *10*, 316.  
 (34) Aquino, A. A.; Mulcahy, C. P. A.; Jones, T. S. *Surf. Sci. Lett.* **1995**, *344*, L1231.

H<sub>2</sub>, and 24 hydrocarbon compounds ranging from C<sub>1</sub> to C<sub>4</sub>. It also includes pressure and third-body dependencies for the lighter-molecular-weight species. The numbers in Table 3 under the C<sub>a</sub> subheadings refer to the reactions listed in Table 2 of Marinov et al.<sup>21</sup> Additional reactions presented in Table 3 are recent enhancements<sup>38</sup> or modifications<sup>39</sup> to the original work and thereby indicate where G1 deviates from the published version of the Marinov mechanism. In the interest of limiting this discussion to TMI<sub>n</sub>, the reader is referred to Marinov for more information regarding this extensive hydrocarbon combustion mechanism.

The final reaction sequence (labeled BLS in Table 3) is a combination of G1 and a series of gas-phase reactions between H, CH<sub>3</sub>, and HIn(CH<sub>3</sub>)<sub>3</sub> that were proposed by Buchan et al.<sup>7</sup> These authors invoked the existence of a gas-phase hypervalent indium compound (HIn(CH<sub>3</sub>)<sub>3</sub>) in order to explain their experimental observations. The BLS reactions do not form a sound kinetic model because, in all likelihood, H abstraction by H or CH<sub>3</sub> from TMI<sub>n</sub> would result in the production of H<sub>2</sub> or CH<sub>4</sub> along with a methylene-like species of the form CH<sub>2</sub>In(CH<sub>3</sub>)<sub>2</sub>, rather than a hypervalent compound. In addition, the unimolecular decomposition of HIn(CH<sub>3</sub>)<sub>3</sub> is not microscopically reversible. However, the mechanism proposed by Buchan can be considered general in the sense that all gas-phase processes in this system that result in the decomposition of TMI<sub>n</sub> must involve H and CH<sub>3</sub>. Regardless of the byproducts, BLS can be used to test the validity of a generic gas-phase radical process under the influence of various carrier gas mixtures.

The model chemistry listed in Tables 2 and 3 provides a functional platform from which to evaluate the relative effects of carrier-gas composition on TMI<sub>n</sub> pyrolysis chemistry in flow-tube reactors. The kinetic parameters (*A*, *β*, and *E*) used to calculate sticking coefficients for the reactions listed in S1, S2, and S3 were fit to TMI<sub>n</sub> conversion rates that were measured during the current investigation, as well as from previous flow-tube work conducted in our laboratory.<sup>13</sup> The stoichiometric variable *x* in these equations determines the relative amount of incident carbon that desorbs as CH<sub>3</sub> per unit of TMI<sub>n</sub> converted. For each set of simulations, *x* was varied from a minimum of 0, corresponding to no CH<sub>3</sub> desorption, to a maximum of 3, which forces all incident carbon to desorb as CH<sub>3</sub>. Comparing model predictions of hydrocarbon product distributions for different values of *x* to experimental observations is a valuable tool for distinguishing between dominant chemical pathways. The Arrhenius parameters for the reactions listed in G1 and BLS were taken directly from their respective literature sources without modification.

Illustrated in Figures 6 and 7 are the mole fractions of CH<sub>4</sub> and C<sub>2</sub>H<sub>6</sub> predicted by CRESLAF as a function of the incident carbon fraction that desorbs as CH<sub>3</sub>. This fraction (*y*) is simply related to *x* by the expression: *y* = *x*/3. As indicated in the legends of each graph, the open symbols denote model results for different combinations of surface and gas-phase reaction mechanisms. The crosshatched bars in each figure are the measured

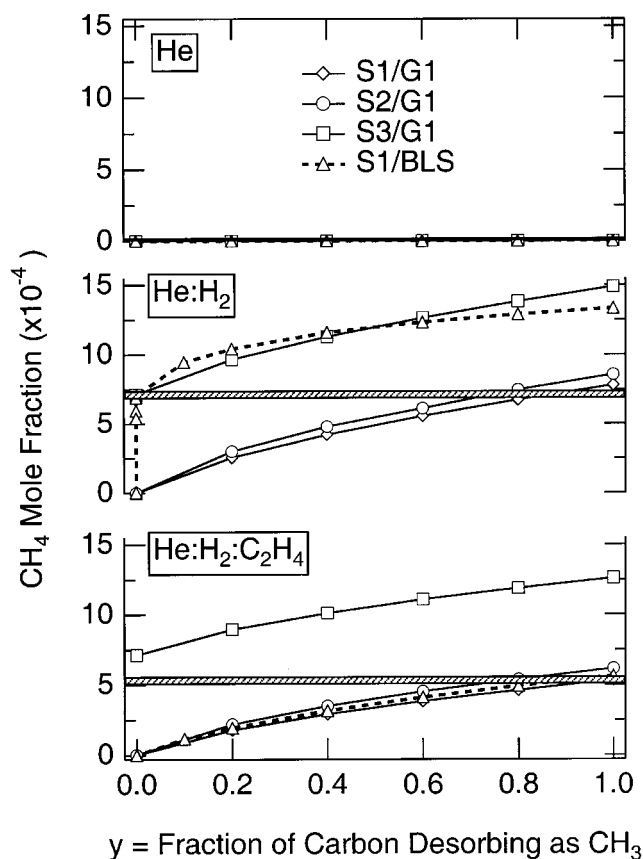


**Figure 6.** Mole fraction of CH<sub>4</sub> predicted by CRESLAF as a function of the incident carbon that desorbs from the surface as CH<sub>3</sub> radical. The crosshatched bars indicate upper and lower error bounds of the measured value. [S1/G1], [S2/G1], [S3/G1], and [S1/BLS] are model predictions for different combinations of gas-phase and surface reaction mechanisms (see text).

mole fractions bounded by the respective experimental uncertainties. Data presented in the uppermost graphs reflect the product distributions for TMI<sub>n</sub> decomposition in pure He carrier gas. The middle and lower graphs in Figures 6 and 7 illustrate the effects induced by adding H<sub>2</sub> and C<sub>2</sub>H<sub>4</sub> to the simulated chemistry, respectively.

**Carrier Gas Effects.** In general, the predictions of each of the proposed mechanisms are consistent with experimental observations in that CH<sub>4</sub> is a byproduct of adding H<sub>2</sub> to the carrier gas. This behavior is evidenced by the uppermost graph of Figure 6, in which all four mechanisms predict no CH<sub>4</sub> formation in pure He. Also, the relative amounts of CH<sub>4</sub> and C<sub>2</sub>H<sub>6</sub> formed in either H<sub>2</sub> or H<sub>2</sub>:C<sub>2</sub>H<sub>4</sub> ambients are dependent upon the fraction of incident carbon desorbed as CH<sub>3</sub>, with more CH<sub>4</sub> and consequently less C<sub>2</sub>H<sub>6</sub> produced at larger values of *y*. In addition, a trend in the simulation results has emerged for the fraction desorbed as CH<sub>3</sub>; the model predictions are most accurate at either large (*y* = *x*/3 ≥ 0.8) or small (*y* = *x*/3 ≤ 0.05) fractions, but not intermediate.

Focusing on the transition from He to a 50:50 mixture of He:H<sub>2</sub> (upper two graphs in Figures 6 and 7), it appears that mechanisms S3/G1 and S1/BLS are more consistent with experimental observation than either S1/G1 or S2/G1. Reaction set S1/G1 is valid in He carrier gas but fails to predict adequate amounts of C<sub>2</sub>H<sub>6</sub> at large *y*, or CH<sub>4</sub> at small *y*, in the presence of H<sub>2</sub>. This is

(38) Marinov, N. M. *Personal communication*, 1999.

(39) Fahr, A.; Laufer, A.; Klein, R.; Braum, W. *J. Phys. Chem.* **1991**, *95*, 3218.



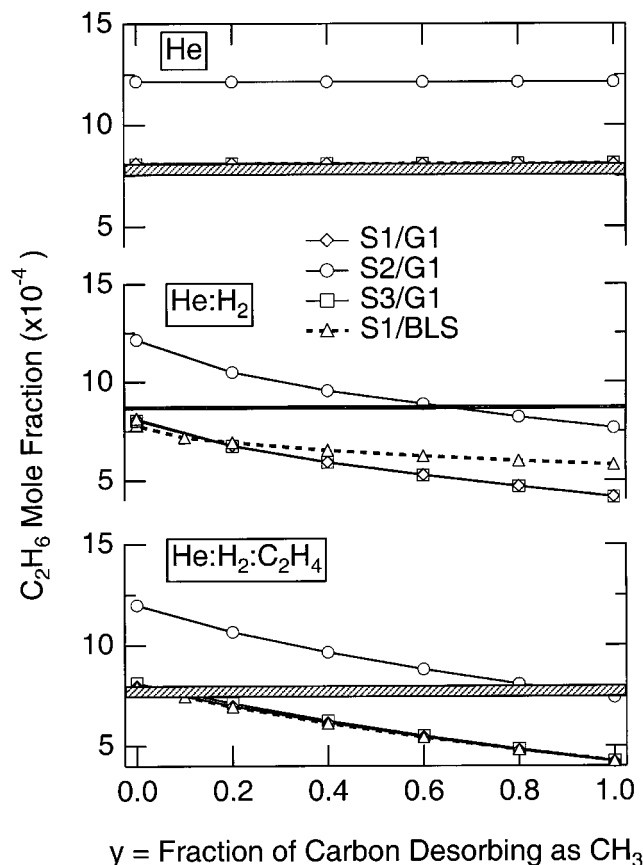


**Figure 7.** Mole fraction of  $C_2H_6$  predicted by CRESLAF as a function of the incident carbon that desorbs from the surface as  $CH_3$  radical. The crosshatched bars indicate upper and lower error bounds of the measured value. [S1/G1], [S2/G1], [S3/G1], and [S1/BLS] are model predictions for different combinations of gas-phase and surface reaction mechanisms (see text).

primarily due to a lower steady-state conversion of TMI<sub>n</sub> that is carrier-gas independent in this mechanism. In essence, there are no alternate routes for organometallic decomposition in S1/G1 that become active under  $H_2$ . Conversely, S2/G1 is valid for He: $H_2$  mixtures (at  $y = 0.80$ ), yet overpredicts the amount of  $C_2H_6$  formed in pure He because conversion of TMI<sub>n</sub> is too high. The only difference between these two scenarios is a 2 kcal mol<sup>-1</sup> change in the activation energy for the global surface reaction. If it were possible for  $H_2$  to increase the reactivity of the surface by lowering the energy barrier 2 kcal mol<sup>-1</sup> without affecting other aspects of the chemistry, then these two mechanisms (S1/G1 and S2/G1) combined would be valid. Additionally, S1/G1 and S2/G1 predict that a substantial portion of the incident carbon ( $y = 0.80$ ) desorbs into the gas as  $CH_3$  during decomposition.

Reaction sets S3/G1 and S1/BLS most accurately reflect the change in hydrocarbon product distributions as the carrier gas composition moves from He to a mixture of He: $H_2$ . Both mechanisms also predict that very little  $CH_3$  ( $y \leq 0.05$ ) needs to desorb from the surface in order to explain the product mixing ratio. What is most interesting about these two scenarios is that S3/G1 does not rely heavily on gas-phase radical reactions for either  $CH_4$  or  $C_2H_6$  formation at small values of  $y$ , whereas the  $CH_4$  production from S1/BLS is entirely homogeneous. As a result of these differences,

the validity of either mechanism may be distinguished by changing the chemical content of the gas-phase radical pool (e.g., by adding  $C_2H_4$ ).

**Ethylene Addition.** The effects of  $C_2H_4$  addition on the hydrocarbon product distributions are illustrated in the lower plots of Figures 6 and 7. Experimentally, the changes observed are relatively minor, with  $CH_4$  production dropping by 25%,  $C_2H_6$  production by 11%, and TMI<sub>n</sub> conversion by 7% from carrier-gas mixtures of He: $H_2$  to He: $H_2$ : $C_2H_4$  (see Table 1 and Figure 5).  $C_2H_4$  effectively competes with  $H_2$  for H and  $CH_3$ , thereby creating longer chain alkyls such as  $C_3H_6$ ,  $C_3H_8$ , and  $C_4H_{10}$ , which make  $CH_4$  and  $C_2H_6$  formation slightly less favorable. Therefore, we can surmise at the outset that mechanisms which promote substantial gas-phase reactions involving H and  $CH_3$  would be more influenced by  $C_2H_4$  than ones that do not.

All of the S<sub>a</sub>/G1 ( $a = 1, 2, 3$ ) mechanisms behave as expected in the presence of  $C_2H_4$ . We observe that S1/G1 and S2/G1 are more sensitive to a change in carrier-gas composition than S3/G1 because the former reaction schemes necessitate 80% of the incident carbon desorb as  $CH_3$ , as opposed to the latter which dictates a much smaller percentage. Under the influence of  $C_2H_4$ , S2/G1 is better overall at predicting the decrease in  $CH_4$  and  $C_2H_6$  than either S1/G1 or S3/G1. In fact, the model predictions for S3/G1 in He: $H_2$ : $C_2H_4$  are essentially identical to those in He: $H_2$  because so little of the incident carbon leaves the surface as a reactive intermediate.

The same is not true for the S1/BLS reaction scheme. Even though  $y$  is less than 0.05, the data in Figure 6 show a substantial decrease in the  $CH_4$  mole fractions from He: $H_2$  to He: $H_2$ : $C_2H_4$  carrier-gas mixtures. This drop in  $CH_4$  production is accompanied by a 30% decrease in the predicted steady-state conversion of TMI<sub>n</sub>. In the S1/BLS model,  $C_2H_4$  completely negates the enhanced decomposition of TMI<sub>n</sub> induced by  $H_2$  addition and therefore is not substantiated by experimental observation, which indicates only a 7% change in the steady-state TMI<sub>n</sub> conversion (see Table 1 and Figure 5). In this case, the simulations predict that  $C_2H_4$  reduces the gas-phase H-atom concentration by 4 orders of magnitude and thereby eliminates the interaction between H and TMI<sub>n</sub>. In turn, this prevents the formation of hypervalent trimethylindium hydride and the subsequent process of TMI<sub>n</sub> decomposition and  $CH_4$  production. Of all the mechanisms tested, S1/BLS is clearly the most sensitive to the addition of ethylene and least supported by experimental observation.

**Summary of Numerical Experiments.** Four separate reaction mechanisms (presented in Tables 2 and 3) were assembled and tested in order to identify major pathways that govern the heterogeneous decomposition of TMI<sub>n</sub> in hot-wall flow-tube reactors. The mechanisms were incorporated into a two-dimensional boundary-layer code used to simulate the effects of carrier-gas composition on the steady-state hydrocarbon product distribution and the conversion efficiency of TMI<sub>n</sub>.

The simulations of  $C_2H_4$  addition conclusively demonstrate that gas-phase reactions proposed by Buchan et al. cannot account for the acceleration of TMI<sub>n</sub> decomposition in  $H_2$  carrier gas. Moreover, it is unlikely that gas-phase reactions of *any* kind play a substantial

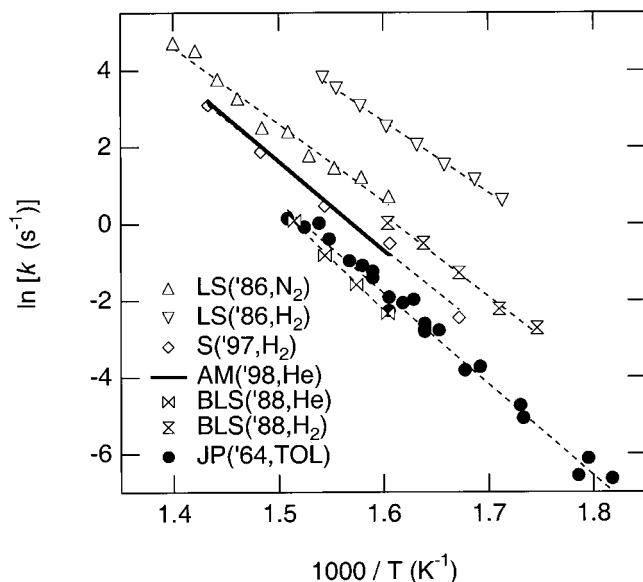


**Figure 8.** Arrhenius plot for the pyrolysis of TMIn comparing previously published results taken under steady-state conditions in flow-tube reactors. LS = Laresen and Stringfellow,<sup>6</sup> S = Sigiyama et al.,<sup>8</sup> AM = Allendorf and McDaniel,<sup>13</sup> BLS = Buchan, Larsen, and Stringfellow,<sup>7</sup> and JP = Jacko and Price.<sup>5</sup>

role in the thermal decomposition of TMIn at temperatures below 673 K. We believe there is a small presence of CH<sub>3</sub> in the boundary layer above the active surface; however, the chemistry that ensues from this reactive intermediate accounts for less than 10% of the hydrocarbon products and does not influence the rate of TMIn decomposition under the conditions of our experiments. Completely surface-mediated processes, such as those incorporated into mechanism S3, that result in the adsorption of TMIn and H<sub>2</sub>, followed by desorption of CH<sub>4</sub> and C<sub>2</sub>H<sub>6</sub>, appear to be the most important pathways for thermal decomposition of TMIn in hot-wall flow-tube reactors.

## V. Discussion and Conclusions

The experiments reported here demonstrate that TMIn pyrolysis in hot-wall flow-tube reactors can be classified as an autocatalytic process. The presence of an induction or incubation period that is thermally activated, followed by an exponential increase in the consumption rate of the organometallic, is behavior consistent with similarly classified metal-deposition reactions of iron,<sup>40</sup> platinum,<sup>41</sup> and tungsten.<sup>42</sup> After activation of the reactor walls, TMIn decomposition achieves a self-limited, time-invariant conversion rate that can be fit to a first-order kinetic expression. This fact is evident in Figure 8, which is an Arrhenius plot of the rate constant for pyrolysis measured by all previous investigators, including recent work from this laboratory,<sup>13</sup> at a variety of pressures and carrier-gas compositions. All of the aforementioned investigations used hot-wall flow-tube reactors and collected data

under steady-state conditions in *seasoned* vessels. The result is a mutually consistent body of work, with a first-order rate constant that varies over 2.6 orders of magnitude, but yields an average activation energy for reaction 1 of  $44 \pm 6$  kcal mol<sup>-1</sup>.

Unfortunately, it is not uncommon for entirely heterogeneous systems to behave in a first-order manner, yielding observations identical to those expected for a unimolecular decomposition. In this instance, it can be very difficult to distinguish between homogeneous and heterogeneous chemistries, due to a complex coupling between the two phenomena.<sup>43–45</sup> In fact, the inability to resolve individual contributions of gas and surface reactions on the observed behavior can invalidate the experimental approach altogether. This seems to be the case for TMIn pyrolysis in hot-wall flow-tube reactors, where the contributions of heterogeneous processes have been overlooked, leading to an underestimation of the bond strengths in TMIn and the belief that this reaction is entirely homogeneous.

The carrier-gas effects observed in this system are not uncommon to thin-film MOCVD processes. There are numerous instances in the literature that describe an increase in the deposition rates for Al,<sup>46</sup> Cu,<sup>47</sup> GaN,<sup>24,48</sup> and CdTe,<sup>49</sup> upon substitution of H<sub>2</sub> for inert carrier gases. In addition to increased film growth rates, these papers have noted a dramatic change in the physical properties of the resulting solid, such as improved morphology and smaller grain sizes, better conformal coverages, and lower film resistivities. It is unclear the extent to which gas-phase reactions are responsible for the observations in these systems. For TMIn, however, our numerical work suggests a strong heterogeneity associated with the H<sub>2</sub> chemistry. The simulation results essentially eliminate the likelihood that, at temperatures below 673 K, gas-phase processes either contribute to the thermal decomposition of TMIn or are responsible for a significant fraction of the CH<sub>4</sub> formed under H<sub>2</sub>.

The most significant result of this work is the realization that hot-wall flow-tube reactors are inappropriate for investigating pyrolysis of TMIn. It may be possible to generalize this conclusion to include gallium and possibly aluminum organometallic compounds as well. In looking at TMGa, which is another important group IIIA compound that has been investigated with flow reactors,<sup>50–52</sup> there are striking similarities to the TMIn system. In particular, investigators have observed carrier-gas effects and have reported different energetics and decomposition rates that are dependent upon the surfaces within the reactor. In addition, recent published results of high-level theoretical calculations now

(43) Brown, R. L. *J. Res. Natl. Bur. Stand.* **1978**, *83*, 1.

(44) Howard, C. J. *J. Phys. Chem.* **1979**, *83*, 3.

(45) Orkin, V. L.; Khamaganov, V. G.; Larin, I. K. *Int. J. Chem. Kinet.* **1993**, *25*, 67.

(46) Yun, J. H.; Rhee, S. W. *J. Mater. Sci.* **1998**, *9*, 1.

(47) Kim, S.; Park, J. M.; Choi, D. *J. Thin Solid Films* **1998**, *315*, 229.

(48) Schon, O.; Schineller, B.; Heuken, M.; Beccard, R. *J. Cryst. Growth* **1998**, *190*, 335.

(49) McDaniel, A. H.; Wilkerson, K. J.; Hicks, R. F. *J. Phys. Chem.* **1995**, *99*, 3574.

(50) Jacko, M. G.; Price, S. J. W. *Can. J. Chem.* **1963**, *41*, 1560.

(51) Larsen, C. A.; Buchan, N. I.; Stringfellow, G. B. *Appl. Phys. Lett.* **1988**, *52*, 480.

(52) Hoshino, M. *J. Appl. Phys.* **1990**, *68*, 2538.

(40) Kellerman, B. K.; Chason, E.; Adams, D. P.; Mayer, T. M.; White, J. M. *Surf. Sci.* **1997**, *375*, 331.

(41) Xue, Z.; Thridandam, H.; Kaesz, H. D.; Hicks, R. F. *Chem. Mater.* **1992**, *4*, 162.

(42) McConica, C. M.; Cooper, K. *J. Electrochem. Soc.* **1988**, *135*, 1003.

suggest that the experimentally determined bond energies for TMGa are too low by 10–15 kcal mol<sup>-1</sup>.<sup>14,53,54</sup> The kinetic data extracted from the early flow reactor experiments of Jacko and Price and others for TMIn and TMGa have been used extensively by subsequent investigators in formulating mechanistic arguments for MOCVD of groups IIIA–VA materials.<sup>2,54</sup> The results

---

(53) Trachtman, M.; Beebe, S.; Bock, C. W. *J. Phys. Chem.* **1995**, *99*, 15028.

(54) Simka, H.; Willis, B. G.; Lengyel, I.; Jensen, K. F. *Prog. Crystal Growth Charact.* **1997**, *35*, 117.

of this investigation would suggest that conclusions based upon these earlier works should be reexamined.

**Acknowledgment.** The authors are grateful for the support of this research provided by Libbey-Owens-Ford Co. (Toledo, OH) and the U.S. Department of Energy, Office of Industrial Technologies, Advanced Industrial Materials Program.

CM990497F